Intracellular formate is a critical mediator of the antimicrobial fate of *Salmonella* Typhimurium Against meropenem and ciprofloxacin

Debapriya Mukherjee[1], Sakshi Vasant Wagle[2], Pallab Ghosh[1#], Abhishek Biswas[1#], Dipshikha Chakravortty[1,3*]

[1]Department of Microbiology and Cell Biology, Division of Biological Sciences, Indian Institute of Science, Bangalore, India.

[2]Department of Biological Sciences, Indian Institute of Science Education and Research, Bhopal, India

[3]School of Biology, Indian Institute of Science Education and Research, Thiruvananthapuram, 695551.

#Equal contribution

[*]Corresponding author: dipa@iisc.ac.in

Tel: 0091 80 2293 2842

Fax: 0091 80 2360 2697

Abstract

The emergence of multidrug-resistant *Salmonella enterica* serovar Typhimurium (STM) poses a critical threat to global health. While classical antimicrobial resistance (AMR) mechanisms are well-characterized, alternative metabolites and metabolic pathways also contribute to resistance. This study highlights the role of intracellular formate, maintained by pyruvate-formate lyase (PflB), in modulating susceptibility of STM to meropenem and ciprofloxacin. Loss of *pflB* disrupts intracellular pH (ipH), impairing efflux pump activity, increasing reactive oxygen species (ROS), and causing membrane depolarization. These effects enhance antibiotic susceptibility but are reversed by extracellular formate supplementation. Mechanistically, disrupted ipH activates the RpoE–*csrB* axis, leading to downregulation of efflux pump genes *acrB* and *tolC*. Additionally, the BarA/SirA two-component system can also modulate the pathway. Our findings uncover a non-canonical role of formate in regulating efflux-mediated AMR, emphasizing its potential as a metabolic target in combating resistant STM strains.

Keywords: PflB, Antimicrobial response (AMR), Efflux pumps, CsrA/*csrB* axis

Introduction

48 The widespread misuse and overuse of antibiotics over recent decades have substantially
49 contributed to the accelerated emergence of bacterial antimicrobial resistance (AMR) [1, 2].
50 Among resistant pathogens, multidrug-resistant (MDR) *Salmonella* has emerged as a
51 significant global health concern due to its association with elevated morbidity and mortality
52 rates. In 2019, AMR-related *Salmonella* infections were estimated to have caused
53 approximately 1,50,000 deaths worldwide, with 23,700 cases directly attributable to MDR
54 strains [3]. *Salmonella enterica* subspecies *enterica* serovar Typhimurium (STM) is one of the
55 most prevalent serotypes implicated in MDR infections and plays a critical role in the declining
56 efficacy of commonly used antibiotics, posing a substantial threat to public health systems
57 globally [4-7].

58 *Salmonella* employs a range of mechanisms to evade antibiotic action, including enzymatic
59 degradation of antibiotics, efflux pump-mediated drug expulsion, structural modification of
60 antimicrobial agents, and alteration or protection of drug targets[8, 9]. While these resistance
61 strategies have been well characterized in recent studies, the role of bacterial metabolism in
62 modulating antimicrobial resistance (AMR) in *Salmonella* remains underexplored. In our
63 previous work, we elucidated the role of the *pflB* gene—encoding pyruvate-formate lyase
64 (PflB)—in STM pathogenesis. PflB contributes to the maintenance of the intracellular pool of
65 formate, a short-chain fatty acid that plays a critical role in regulating intracellular pH (ipH).
66 In the *pflB* deletion mutant (STM Δ*pflB*), dysregulation of ipH results in membrane
67 perturbation, activation of the extra cytoplasmic sigma factor RpoE, increased expression of
68 the small RNA *csrB*, and subsequent repression of flagellar gene expression[10]. Further, in a
69 serendipitous finding in our laboratory, we observed that deletion of *pflB* also sensitizes STM
70 to the antibiotics meropenem and ciprofloxacin. This unexpected finding prompted a detailed
71 investigation into the role of intracellular formate homeostasis in AMR regulation.

72 In this study, we investigated the role of both the intracellular formate pool and extracellular
73 formate supplementation in modulating antibiotic resistance in STM and evaluated their
74 potential as novel therapeutic targets. Our findings indicate that membrane damage resulting
75 from dysregulated intracellular pH (ipH) in STM influences the expression of the efflux pump
76 *acrB* through activation of the sigma factor RpoE. Additionally, extracellular formate
77 supplementation leads to downregulation of *acrB* expression via the BarA/SirA-regulated
78 CsrA/*csrB* regulatory pathway. To the best of our knowledge, this is the first report
79 demonstrating the impact of intracellular formate levels on antibiotic susceptibility in STM,
80 and how intracellular and extracellular formate pools distinctly modulate its antimicrobial
81 response.

82

83 ## Materials and Methods

84 ### Bacterial strains and culture conditions

85 The wild-type *Salmonella enterica* subsp. *enterica* serovar Typhimurium strain 14028S used
86 in this study was kindly provided by Professor Michael Hensel (Max von Pettenkofer Institute
87 for Hygiene and Medical Microbiology, Germany). All bacterial strains were preserved as
88 glycerol stocks at −80 °C and revived on Luria-Bertani (LB) agar plates (HiMedia)
89 supplemented with the appropriate antibiotics when necessary (50 µg/ml kanamycin, 50 µg/ml
90 ampicillin, or 25 µg/ml chloramphenicol). Single colonies were inoculated into LB broth
91 supplemented with the appropriate antibiotics and incubated overnight at 37 °C with shaking
92 at 170 rpm. The overnight cultures were then diluted 1:100 in fresh LB medium and grown
93 under the same conditions for 6 hours to obtain bacteria in the logarithmic growth phase. The
94 optical density at 600 nm (OD_{600}) was subsequently adjusted to 0.1 in Mueller-Hinton Broth
95 (MHB), corresponding to approximately 10^6 colony-forming units (CFU), for use in

96 downstream experiments. A detailed list of bacterial strains and plasmids used in this study is
97 provided in Table 1.

98 **Table 1**

Bacterial strains/plasmids	Characteristics	Source
Salmonella enterica subspecies *enterica* serovar Typhimurium strain 14028S	Wild type	Gift from Prof. M. Hensel
STM Δ*pflB*	Kan^R	Laboratory stock
STM Δ*pflB*/pQE60*: pflB*	Kan^R, Amp^R	Laboratory stock
STM Δ*fliC*	Kan^R	Laboratory stock
STM Δ*rpoE*	Chl^R	Laboratory stock
STM Δ*pflB*Δ*rpoE*	Kan^R, Chl^R	Laboratory stock
STM Δ*sirA*	Chl^R	Laboratory stock
STM Δ*pflB*Δ*sirA*	Kan^R, Chl^R	Laboratory stock
pQE60	Low copy number plasmid, Amp^R	Laboratory stock

99

100 **Determination of MIC of meropenem, ciprofloxacin, ceftazidime**

101 Logarithmic phase bacterial cultures, adjusted to an OD_{600} of 0.1, were inoculated into 96-well
102 microtiter plates containing Mueller-Hinton Broth (MHB) supplemented with serial dilutions
103 of antibiotics. The concentrations used were as follows: meropenem (8 to 0.0156 mg/L)
104 (Sigma), ciprofloxacin (0.5 to 0.0009 mg/L) (Sigma), and ceftazidime (128 to 0.125 mg/L).
105 Plates were incubated at 37 °C with shaking at 170 rpm for 14-16 hours. Bacterial growth was
106 assessed by measuring OD_{600} using a Tecan microplate reader.

107 **Estimation of bacterial viability using resazurin assay**

108 Following antibiotic exposure and incubation for 14-16 hours, 20 µL of resazurin solution
109 (prepared from a 0.2 mg/mL stock) was added to each well and incubated for 2 hours in the
110 dark. Thereafter, fluorescence intensity was measured using a Tecan microplate reader with
111 excitation at 540 nm and emission at 590 nm. Cell viability was determined based on
112 fluorescence and expressed as a percentage of untreated controls.

113 **Flow cytometry mediated quantification of live/dead population, intracellular reactive**
114 **oxygen species (ROS), membrane depolarization, and ipH**

115 After 14–16 hours of antibiotic treatment, bacterial cells were stained with a panel of
116 fluorescent dyes: Propidium Iodide (PI, 1 µg/mL) for live/dead discrimination,
117 dichlorodihydrofluorescein diacetate (DCF_2DA, 10 µM) to assess intracellular reactive oxygen
118 species (ROS), Bis-(1,3-Dibutylbarbituric Acid) Trimethine Oxonol ($DiBAC_4$, 1 µg/mL) for
119 measuring membrane depolarization, and 2′,7′-Bis-(2-Carboxyethyl)-5-(and-6)-
120 Carboxyfluorescein Acetoxymethyl Ester (BCECF-AM, 20 µM) for intracellular pH (ipH)
121 comparison. Stained samples were incubated in the dark for 15 minutes and subsequently
122 analyzed using the BD FACSVerse flow cytometer (BD Biosciences, USA). Data including dot
123 plots, density plots, median fluorescence intensity (MFI), and the percentage of positively
124 stained cells were acquired and processed using BD FACSVerse software.

125

126 **RNA isolation and RT-qPCR**

127 Logarithmic-phase bacterial cultures were harvested by centrifugation at 6,000 rpm for 10
128 minutes at 4 °C, and the resulting cell pellets were resuspended in TRIzol reagent. Samples
129 were stored at −80 °C until further processing. Total RNA was extracted using the chloroform–
130 isopropanol method, and RNA pellets were washed with 70% ethanol and resuspended in 30 µL

131 of DEPC-treated Milli-Q water. RNA concentration was measured using a NanoDrop
132 spectrophotometer (Thermo Fisher Scientific), and RNA integrity was verified by
133 electrophoresis on a 2% agarose gel. For removal of genomic DNA, 2 µg of total RNA was
134 treated with TURBO DNase (Thermo Fisher Scientific) at 37 °C for 30 minutes, followed by
135 inactivation with 5 mM Na_2EDTA at 65 °C for 10 minutes. First-strand cDNA synthesis was
136 performed using the PrimeScript RT reagent kit (Takara, Cat. No. RR037A) according to the
137 manufacturer's protocol. Quantitative real-time PCR (qRT-PCR) was carried out using the TB
138 Green RT-qPCR kit (Takara) on a QuantStudio 5 Real-Time PCR System. Gene expression was
139 analysed using intragenic primers and normalized to *16S rRNA* levels. Primer sequences are
140 provided in Table 2.

141 **Table 2**

Primer name	**Sequence (5'-3')**
16S *rRNA* RT FP	GTGAGGTAACGGCTCACCAA
16S *rRNA* RT RP	TAACCGCAACACCTTCCTCC
acrB RT FP	CTCTATCACCATCGTATCGG
acrB RT RP	AGTAATCCGTGACCTCATCC
tolC RT FP	TAACGAAGCGCGTAGTCCTT
tolC RT FP	AGCACATCAATAGCGTTCA
ompF RT FP	TGAATCCTATACCGATATGG
ompF RT RP	CCTGCTGATCGTTAGTACGC
emrB RT FP	TGGCGTATCCAGCAGCCTGA
emrB RT RP	GATGCCAATCACCAGTAGCG

142

143

144 **Efflux pump activity by Nile Red Assay**

145 Efflux pump activity was quantified following the method outlined by Lyu *et al*[11]. In brief,
146 bacterial cultures in the logarithmic growth phase were adjusted to an optical density of 0.1 at
147 600 nm (OD_{600}). A volume of 100 µl from each normalized culture was dispensed into wells of
148 a 96-well microplate and incubated with Nile Red dye at a final concentration of 48 µg/ml. The
149 plate was incubated in the dark under shaking conditions for 3 hours. Fluorescence
150 measurements were then obtained using a TECAN microplate reader, with excitation and
151 emission wavelengths set at 549 nm and 628 nm, respectively. Fluorescence intensity values
152 were normalized against absorbance readings at 600 nm.
153

154 **Atomic Force Microscopy**

155 After 14–16 hours of antibiotic exposure, bacterial cells were drop-cast onto sterile glass
156 coverslips. Once air-dried, the cells were fixed by treating them with 3.5% paraformaldehyde
157 for 10 minutes. Residual salts were removed by washing the samples three times with double-
158 autoclaved MilliQ water. The coverslips were then dried in a vacuum desiccator prior to
159 imaging with the NX10 Atomic Force Microscope (AFM). Image processing and
160 measurements of cell length and height were performed using XEI software.
161

162 **Animal experiments**

163 All animal experiments were conducted with prior approval from the Institutional Animal
164 Ethics Clearance Committee (IAEC) at the Indian Institute of Science, Bangalore. The institute
165 is registered under CPCSEA with registration number 48/1999/CPCSEA. All procedures
166 strictly adhered to the guidelines set by the Committee for the Purpose of Control and
167 Supervision of Experiments on Animals (CPCSEA). The ethical approval number for this study
168 is CAF/Ethics/853/2021.

169 A modified protocol based on the method described by Roy Chowdhury *et al.* was employed
170 to evaluate the organ burden following infection and antibiotic treatment with the wild-type
171 (WT) and mutant bacterial strains[12]. Briefly, 10^6 cells from overnight cultures were orally
172 gavaged into 6–8-week-old C57BL/6 mice on day 0 (0 dpi). Mice received 1 mg/kg of the
173 respective antibiotics on days 2 and 4 post-infection. On day 5 post-infection, the animals were
174 ethically euthanized, and the intestine, liver, and spleen were collected. These organs were
175 homogenized, and serial dilutions of the homogenates were plated on *Salmonella-Shigella* (SS)
176 agar. Bacterial load was quantified and expressed as $\log_{10}$ CFU per gram of tissue.

177 To compare mortality rates between STM WT and STM Δ*pflB* under antibiotic exposure,
178 groups of mice (n=5) were orally administered 10^6 cells from stationary phase cultures of each
179 strain. Starting from day 2 post-infection, 1 mg/kg of the respective antibiotics was
180 administered every alternate day till the mice survived. Survival was monitored daily and
181 represented as percent survival. A 125 mM solution of sodium formate was supplemented in
182 the drinking water provided to the animals in both experimental setups.

183

184 **Estimation of Formate in mouse serum by Gas Chromatography-Mass Spectrometry**

185 To quantify formate levels in mouse serum following supplementation with 125 mM sodium
186 formate in drinking water, a protocol adapted from Hughes *et al* was employed[13]. Male
187 C57BL/6 mice (6–8 weeks old) were provided with 125 mM sodium formate in their drinking
188 water. At five days post-infection, blood was collected via retro-orbital puncture. After clotting,
189 serum was separated by centrifugation at 10,000 × g for 20 minutes and subsequently used for
190 formate quantification.

191 Sodium formate (Sigma) served as an external standard. Both standards and biological samples
192 were derivatized prior to mass spectrometry analysis. To protonate the formate, 2 M

193 hydrochloric acid was added to each sample in a 1:1 ratio. Liquid-liquid extraction was
194 performed to isolate formic acid into ethyl acetate (Sigma-Aldrich). Residual water was
195 removed by passing the ethyl acetate extract through an anhydrous sodium sulfate column
196 (Sigma-Aldrich). The extract was then incubated at 80 °C for 1 hour with the derivatizing
197 reagent N,O-Bis(trimethylsilyl)trifluoroacetamide (Sigma-Aldrich) containing 1%
198 chlorotrimethylsilane (Fluka). Derivatized samples were transferred to autosampler vials for
199 analysis using Gas Chromatography-Mass Spectrometry (GC-MS; Agilent Technologies,
200 7890A GC, 5975C MS).

201 Injection parameters were as follows: injection temperature of 200 °C, injection split ratio of
202 1:40, and injection volume of 1 µL. The oven temperature program began at 40 °C (held for 4
203 minutes), increased to 120 °C at a rate of 5 °C/min, and then to 200 °C at 25 °C/min, with a
204 final hold of 3 minutes. Helium was used as the carrier gas at a constant flow rate of
205 1.2 mL/min. Chromatographic separation was performed using a 30 m × 0.25 mm × 0.40 µm
206 DB-624 column (Agilent). The interface temperature was maintained at 220 °C, and the
207 electron impact ion source operated at 230 °C with an ionization energy of 70 eV and 1235 EM
208 volts.

209 For qualitative analysis, selected ion monitoring in single quadrupole mode was employed with
210 a scan at m/z 103. The retention time for formate and its deuterated analog was approximately
211 5.9 minutes. The target and reference (qualifier) ions for formate were m/z = 103 and m/z =
212 75, respectively. Sample concentrations were determined by interpolating from a standard
213 calibration curve generated using known concentrations.

214

215 **Determination of the fraction of antibiotic persister**

216 The determination of antibiotic persister was performed by modifying a protocol described by
217 Drescher *et al*[14]. Logarithmic phase cultures of STM WT and STM Δ*pflB* strains were treated
218 with 15X and 25X the minimum inhibitory concentration (MIC) of meropenem (2 and
219 ciprofloxacin. To determine the persister population, aliquots were collected at specified
220 timepoints post-treatment and plated for colony-forming unit (CFU) enumeration. Similarly,
221 24-hour-old biofilm cultures were exposed to the same antibiotic concentrations, and persister
222 cells were quantified via plating. The resulting CFU counts were normalized against the pre-
223 inoculum values to calculate fold viability relative to the 0-hour timepoint. Data were expressed
224 as $\log_{10}$(fold decrease in CFU relative to 0 h).

225

226 **Statistical Analysis**

227 Each experiment was independently repeated between 1 and 12 times, as specified in the figure
228 legends. Statistical analyses were conducted using an unpaired Student's t-test, or two-way
229 ANOVA, as indicated in the respective legends. Data from mouse experiments were analysed
230 using the Mann–Whitney U test. A p-value of less than 0.05 was considered statistically
231 significant. Results are presented as Mean ± SD or Mean ± SEM, as noted in the figure legends.
232 All data analysis and graphical representations were performed using GraphPad Prism version
233 8.4.2.

234

235 ## Results

236 **Deletion of *pflB* enhances susceptibility of STM to meropenem and ciprofloxacin, whereas**
237 **supplementation of extracellular formate also heightens susceptibility of STM to these**
238 **antibiotics**

239 To evaluate the susceptibility of STM Δ*pflB* to meropenem and ciprofloxacin, both the wild-
240 type and mutant strains were exposed to varying concentrations of the antibiotics. The STM
241 Δ*pflB* mutant showed significantly increased sensitivity to meropenem, particularly at
242 concentrations of 1 mg/L and 0.5 mg/L **(Figure 1A)**. While the partial restoration of bacterial
243 growth upon sodium formate supplementation was not statistically significant, it suggests that
244 intracellular formate deficiency may contribute to the heightened sensitivity to meropenem.
245 Interestingly, when formate was added to wild-type cells—despite their intact intracellular
246 formate levels—a significant reduction in survivability was observed under antibiotic stress at
247 the same concentrations. Comparable results were obtained with ciprofloxacin, where
248 statistically significant effects were noted at 0.03125, 0.015625, 0.0078, and 0.0039 mg/L
249 **(Figure 1C)**. These findings were further supported by resazurin assay data **(Figure 1B, D)**.
250 The enhanced susceptibility of STM ΔpflB and its recovery in the presence of sodium formate
251 was also true for ceftazidime, a third generation cephalosporin[15]**(Figure S1)**.
252 To investigate how deletion of *pflB* affects STM's antibiotic susceptibility, we treated
253 logarithmic-phase cultures overnight with sub-lethal doses of meropenem (0.5 mg/L) and
254 ciprofloxacin (0.015625 mg/L)and analyzed Propidium Iodide (PI) uptake via flow cytometry.
255 STM Δ*pflB* showed a higher PI-positive population than wild-type (WT), which was
256 significantly reduced with sodium formate supplementation. In contrast, formate
257 supplementation increased PI-positive cells in WT upon antibiotic exposure **(Figure 2A, B)**.
258 Given that bactericidal antibiotics induce reactive oxygen species (ROS) irrespective of their
259 mechanisms, we assessed intracellular ROS using DCF_2DA staining[16-18]. Consistent with PI
260 staining results, STM Δ*pflB* exhibited elevated DCF_2DA-positive populations under antibiotic
261 stress, which was mitigated by formate. Similarly, formate supplementation increased ROS
262 levels in WT cells exposed to antibiotics **(Figure S2 A, B)**. These findings suggest that loss of

263 *pflB*, and thus intracellular formate, increases STM's susceptibility to meropenem and
264 ciprofloxacin, while exogenous formate to wild-type cells also enhances antibiotic sensitivity.
265

266 **Deletion of *pflB* was associated with a transcriptional downregulation of antibiotic efflux**
267 **pumps, which was also common for formate supplemented in wild-type cells**

268 Previous studies have demonstrated that cytoplasmic acidification is a key factor contributing
269 to antibiotic resistance in *Escherichia coli*[19]. Similarly, work by Panta *et al*. has shown that
270 maintenance of optimal cytoplasmic pH is critical for colistin resistance in various bacterial
271 species, including *S. enterica*[20]. To investigate whether intracellular pH dynamics play a role
272 in antibiotic susceptibility in our system, we exposed bacterial strains to sub-lethal
273 concentrations of meropenem and ciprofloxacin and measured intracellular pH using BCECF-
274 AM, a cell-permeable, dual-excitation ratiometric dye[21] **(Figure 2C)**. A reduced 488/405
275 fluorescence ratio in STM WT cells following antibiotic exposure indicated cytoplasmic
276 acidification under antibiotic stress. Consistent with previous observations, STM Δ*pflB*
277 exhibited a higher baseline 488/405 ratio in the absence of stress, which remained unchanged
278 upon antibiotic treatment, suggesting a resistance to cytoplasmic acidification.
279 Supplementation with sodium formate partially restored the 488/405 ratio in STM Δ*pflB*,
280 indicating a modulatory effect of formate on intracellular pH in the presence of antibiotics.
281 While formate supplementation alone did not significantly alter the intracellular pH of STM
282 WT, an increase in the 488/405 ratio was observed upon antibiotic exposure, further supporting
283 the role of formate in buffering pH under stress conditions.

284 Our previous work demonstrated increased membrane depolarization in STM Δ*pflB* compared
285 to WT cells[10]. Given that antimicrobial peptides exert bactericidal effects via membrane
286 depolarization we hypothesized that the enhanced antibiotic susceptibility of STM Δ*pflB* may
287 be attributable, at least in part, to its depolarized membrane state[22-26]. Notably, membrane

288 depolarization was further exacerbated upon exposure to sub-lethal concentrations of
289 meropenem and ciprofloxacin, while sodium formate partially alleviated this effect in STM
290 Δ*pflB*. In contrast, formate supplementation had no impact on membrane potential in WT cells
291 under unstressed conditions, although increased depolarization was observed upon antibiotic
292 exposure **(Figure S2 C, D)**.
293 Efflux-mediated resistance represents a major mechanism of antibiotic failure in Gram-
294 negative bacteria. *Salmonella* harbors multiple efflux systems, among which the TolC-
295 dependent resistance-nodulation-division (RND) family plays a central role in expelling a
296 broad range of clinically relevant antibiotics[27-30]. As proton motive force (PMF) and pH
297 homeostasis are critical for the functioning of these pumps, and membrane depolarization can
298 disrupt PMF, we hypothesized that the reduced antibiotic efflux in STM Δ*pflB* may stem from
299 impaired PMF[11]. To test this, we employed a nile red efflux assay. STM Δ*pflB* retained
300 significantly higher levels of nile red fluorescence, indicating decreased efflux activity.
301 Formate supplementation reduced nile red retention, suggesting partial restoration of efflux
302 capacity. Similarly, formate-treated STM WT cells exhibited increased nile red fluorescence
303 upon antibiotic exposure, consistent with reduced efflux function **(Figure 2D)**.
304 To determine whether reduced efflux activity was due solely to membrane depolarization or
305 also involved transcriptional regulation, we measured mRNA levels of *acrB* and *tolC*, two key
306 components of the RND efflux system in *Salmonella*[31]. Deletion of *pflB* resulted in
307 transcriptional downregulation of both genes, with partial recovery upon formate
308 supplementation. Interestingly, formate supplementation in STM WT also led to reduced *acrB*
309 and *tolC* expression **(Figure 2 E, F)**. These findings suggest that while membrane
310 depolarization may directly impair efflux pump activity, additional transcriptional regulatory
311 mechanisms may also contribute to reduced efflux and heightened antibiotic susceptibility.
312 Outer membrane proteins (Omps) have been linked to antibiotic susceptibility in *Salmonella*,

313 with reduced expression of the large porin OmpF commonly associated with resistance[21, 32, 33].
314 Interestingly, we observed downregulation of *ompF* in STM Δ*pflB* **(Figure 2G)**, despite its
315 increased antibiotic sensitivity. This suggests that the heightened susceptibility in STM Δ*pflB*
316 occurs independently of Omps.
317
318 **Formate supplementation in drinking water and intrabacterial formate deficiency both**
319 **enhanced bacterial clearance by antibiotics *in-vivo***
320 To investigate whether our *in-vitro* findings held true in an *in-vivo* setting, we administered 10^6
321 CFU of STM WT and STM Δ*pflB* orally to C57BL/6 mice. Alongside this, the mice received
322 125 mM sodium formate in their drinking water **(Figure 3A)**. Previous studies have estimated
323 that mice require approximately 40 mmol of formate daily. Given that C57BL/6 mice typically
324 consume around 30 ml of water per day, a 1 M concentration would theoretically be necessary
325 to meet this demand. However, prior research has indicated that providing 500 mM sodium
326 formate in drinking water can lead to weight loss in mice. Therefore, we chose a safer
327 concentration of 125 mM, which corresponds to about 10% of the estimated daily requirement,
328 to stay within physiological limits[34]. In our pilot study, this supplementation level was
329 sufficient to significantly elevate serum formate levels by 5 days post-infection (dpi) **(Figure**
330 **S3)**.
331 Our results showed that combining formate supplementation with meropenem treatment led to
332 a greater reduction in bacterial load compared to meropenem alone, across the intestine, liver,
333 and spleen of C57BL/6 mice. Consistent with earlier findings, the STM Δ*pflB* mutant exhibited
334 a lower organ burden[10]; however, formate supplementation did not restore its bacterial counts.
335 Meropenem further suppressed bacterial levels, and, contrary to our *in-vitro* findings, formate
336 in the drinking water did not rescue the reduced bacterial numbers. Notably, combining formate
337 with meropenem did not lead to a reduction in organ colonization for STM Δ*pflB* as seen in the

338 STM WT, suggesting that STM Δ*pflB* may utilize extracellular formate to support survival
339 under antibiotic pressure **(Figure 3B)**. Similar patterns were observed with ciprofloxacin
340 treatment in STM WT and STM Δ*pflB*-infected mice **(Figure 3C)**. These findings were further
341 corroborated with ceftazidime exposure, where comparable effects were observed in mice
342 infected with STM WT and STM Δ*pflB* under formate-supplemented conditions **(Figure 3D)**.
343

344 **Deletion of *rpoE* from STM Δ*pflB* reversed the enhanced antibiotic susceptibility,**
345 **associated with a recovery in the transcript levels of *acrB* and *tolC***

346 In our previous work, we demonstrated that deletion of *pflB* disrupts intracellular pH
347 homeostasis, leading to membrane depolarization. This perturbation activated the
348 extracytoplasmic sigma factor RpoE, which in turn upregulated transcription of the small RNA
349 *csrB*. The *csrB* RNA antagonizes the activity of the global regulator CsrA by direct binding,
350 thereby impairing processes such as flagellar biosynthesis[10]. Notably, CsrA has been shown to
351 stabilize the *acrAB* transcript by interacting with its 5′ untranslated region (UTR)[35]. Given the
352 increased membrane depolarization observed in STM Δ*pflB* upon antibiotic exposure, we
353 hypothesized that RpoE may regulate *acrB* expression indirectly through modulation of the
354 CsrA–*csrB* regulatory circuit.

355 To test this, we exposed the STM Δ*pflB*Δ*rpoE* strain to sublethal concentrations of meropenem
356 and ciprofloxacin. Compared to STM Δ*pflB*, the double knockout exhibited a significantly
357 reduced proportion of propidium iodide (PI)-positive cells **(Figure 4A, B)**. This was
358 accompanied by a decrease in intracellular reactive oxygen species (ROS), as assessed using
359 DCF_2DA staining **(Figure S4A, B)**.
360

361 Interestingly, deletion of *rpoE* in the STM Δ*pflB* background did not restore membrane
362 potential under basal conditions. However, upon antibiotic challenge, we observed a significant

363 reduction in $DiBAC_4$-positive cells, indicative of partial recovery in membrane polarization
364 **(Figure S4C, D)**. The improved viability of STM Δ*pflB*Δ*rpoE* relative to STM Δ*pflB* under
365 antibiotic stress was further supported by atomic force microscopy, which revealed increased
366 cellular length and height following exposure to both meropenem and ciprofloxacin **(Figure**
367 **S5A, B, C)**.
368 These phenotypic changes correlated with the restoration of *acrB* and *tolC* transcript levels in
369 STM Δ*pflB*Δ*rpoE*, suggesting enhanced efflux activity **(Figure 4C, D)**. This was further
370 confirmed by increased nile red efflux, indicative of improved pump function **(Figure 4E)**.
371 Given the role of EmrB in fluoroquinolone resistance, we also examined its expression **(Figure**
372 **4F)**[36]. As previous studies have not identified a direct regulatory relationship between CsrA
373 and *emrB*, we measured *emrB* transcript levels and observed no significant change in STM
374 Δ*pflB*Δ*rpoE* relative to STM Δ*pflB*. These findings suggest that the observed phenotypic rescue
375 is primarily mediated through the CsrA–*csrB* axis. Deletion of *rpoE* in STM Δ*pflB* led to
376 further downregulation of *ompF*, indicating that while *ompF* suppression does not explain the
377 increased antibiotic sensitivity of STM Δ*pflB*, its further downregulation upon *rpoE* deletion
378 may contribute to the restored resistance observed in STM Δ*pflB*Δ*rpoE* **(Figure 4G)**.
379

380 **Deletion of *sirA* abolishes the antibiotic susceptibility of STM Δ*pflB*, along with reduction**
381 **in ROS levels and membrane depolarization**

382 To further confirm that small RNA *csrB* regulates antibiotic susceptibility, we examined an
383 additional upstream regulator of *csrB*. The BarA/SirA two-component system, which is also
384 known to activate the expression of *csrB* and *csrC* small RNAs, has previously been shown to
385 enhance the expression of HilD, a key regulator of genes within the *Salmonella* Pathogenicity
386 Island-1[37-39]. We deleted *sirA* in the STM Δ*pflB* background and used flow cytometry to
387 quantify propidium iodide-positive cells, revealing a marked reduction in dead cells in the STM

388 Δ*pflB*Δ*sirA* strain compared to STM Δ*pflB* **(Figure 5A, B)**. Interestingly, this decrease in cell
389 death did not correspond with a reduction in membrane depolarization, indicating that the
390 reduced antibiotic sensitivity in STM Δ*pflB*Δ*sirA* was independent of changes in membrane
391 potential **(Figure S6A, B)**. A drop in DCF_2DA-positive cells further supported the observation
392 of diminished antibiotic susceptibility following *sirA* deletion in STM Δ*pflB*. Notably, STM
393 Δ*sirA* alone showed an increase in DCF_2DA-positive cells after exposure to meropenem and
394 ciprofloxacin **(Figure S6 C, D)**. This prompted an investigation into efflux pump expression.
395 We observed that *sirA* deletion in STM Δ*pflB* led to elevated expression of *acrB*, *tolC*, *emrB*,
396 and *ompF* **(Figure 5C, D, E, F)**. A nile red assay confirmed restored efflux pump activity in
397 STM Δ*pflB*Δ*sirA* **(Figure 5G)**. Interestingly, deletion of *sirA* alone resulted in decreased *acrB*
398 transcript levels, which may explain the increased DCF_2DA-positive population upon
399 treatment with meropenem and ciprofloxacin in STM Δ*sirA* **(Figure S6 C, D)**. However, no
400 overall change in efflux activity was detected in STM Δ*sirA*, possibly due to compensatory
401 roles by other efflux pumps **(Figure 5G)**.. These findings suggest that targeting upstream
402 regulators of *csrB* can effectively reverse the antibiotic susceptibility observed in STM Δ*pflB*.
403

404 **Deletion of *pflB* impaired the long-term survival of STM under high antibiotic**
405 **concentrations, a similar effect observed when formate was supplemented to the wild type**
406 Bacterial persistence in the presence of antibiotics, distinct from antibiotic resistance, remains
407 a persistent challenge in effectively eliminating pathogens in clinical settings[40]. Since our data
408 demonstrated that *pflB* deletion increased the antibiotic susceptibility of STM, we aimed to
409 investigate its impact on long-term bacterial survival under high antibiotic stress. Log-phase
410 bacterial cultures, with or without formate supplementation, were exposed to 15× and 25× MIC
411 concentrations of meropenem and ciprofloxacin. Exposure to 15× MIC of meropenem led to a
412 rapid decline in bacterial countsin planktonic culture, with STM Δ*pflB* exhibiting the fastest

413 reduction, reaching statistical significance at 24 hours post-treatment **(Figure 6A)**. Formate
414 supplementation restored survival levels of STM Δ*pflB* to those of the wild type, while
415 supplementation in STM WT also caused a significant reduction in CFUs. Interestingly, by 48
416 and 72 hours, all strains—regardless of formate treatment—showed similar fold decreases in
417 bacterial counts. This effect was specific to planktonic cultures treated with meropenem and
418 was not observed in biofilm forms or in ciprofloxacin-treated planktonic and biofilm cultures
419 **(Figure 6B, C, D)**.
420 Given that the increased susceptibility in earlier experiments was linked to elevated
421 intracellular pH, we examined whether this condition persisted in long-term meropenem-
422 treated cells **(Figure 6E)**. CFUs from 72-hour survivors were stained with BCECF-AM to
423 assess cytosolic acidification. Under untreated conditions, STM Δ*pflB* showed a significantly
424 higher 488/405 fluorescence ratio, indicating elevated intracellular pH. However, after
425 meropenem treatment, all strains—regardless of formate treatment—exhibited similar high
426 levels of cytosolic acidification. These results suggest that intracellular pH plays a key role in
427 bacterial persistence and survival under prolonged, high-dose antibiotic exposure.
428
429

430 Discussion

431 *Salmonella* has become a significant food-borne pathogen exhibiting widespread drug
432 resistance, with the rise of multidrug-resistant strains becoming increasingly concerning[41-43].
433 The growing resistance to existing treatments has complicated clinical management and
434 highlights the urgent need for new antimicrobials or repurposing the existing ones[44, 45].
435 Historically, antimicrobial resistance (AMR) research has largely focused on molecular
436 mechanisms[46, 47]. These include how *Salmonella* and other bacteria resist antibiotics through

437 mechanisms such as modifying antibiotic targets, enzymatic degradation of drugs, and changes
438 in membrane permeability[48-51].
439 More recently, attention has shifted towards the role of bacterial metabolism and metabolic by-
440 products in influencing AMR. For instance, studies have shown that ceftriaxone-resistant
441 *Salmonella* Derby displays altered metabolic activity, particularly in glutathione biosynthesis,
442 with notable decreases in oxidized glutathione and citrulline levels. Supplementing these
443 metabolites externally was found to restore ceftriaxone susceptibility in multidrug-resistant
444 *Salmonella* Derby[52].
445 Several studies have also highlighted the significance of pH in influencing antimicrobial
446 resistance in *Salmonella* and other bacterial species[11, 19, 20, 53]. This underlines the importance
447 of investigating metabolic pathways that are crucial for pH regulation. The enzyme pyruvate-
448 formate lyase (PflB), which catalyzes the conversion of pyruvate into formate and acetyl-CoA,
449 plays a key role in maintaining intracellular pH (ipH)[10]. Consistent with this, our research
450 showed that *Salmonella* Typhimurium lacking *pflB* was more vulnerable to ciprofloxacin and
451 meropenem. Interestingly, this increased susceptibility was partially alleviated by
452 supplementing formate externally.
453 While it is well known that pH affects the proton motive force (PMF), thereby influencing the
454 activity of efflux pumps, our data indicate that pH also regulates efflux pump expression
455 through transcriptional downregulation of *acrB* and *tolC*[11]. In earlier work, we observed that
456 ipH disruption-induced membrane damage activated the RpoE sigma factor, leading to
457 increased expression of the small RNA *csrB*. Deleting *rpoE* reversed the non-flagellated
458 phenotype seen in STM Δ*pflB*[10]. In the current study, we further found that *rpoE* deletion also
459 reversed the increased antibiotic sensitivity of STM Δ*pflB*. A similar effect was seen with the
460 deletion of *sirA*, another upstream regulator of *csrB*. These findings suggest that *pflB* regulates
461 both *Salmonella* invasion and antibiotic resistance through a shared regulatory pathway.

462 Other studies in *E. coli* have demonstrated that adenosine can suppress the stringent response,
463 enhance PMF, promote respiration, and increase antibiotic-induced killing of tolerant and
464 stationary phase persister cells—a phenomenon described as "persister awakening"[54]. Since
465 persistence poses a major hurdle in treating infections, we investigated the long-term survival
466 of STM Δ*pflB* under high-dose antibiotic exposure. In planktonic cultures, STM Δ*pflB*
467 exhibited a faster killing rate than the wild-type, a phenotype reversed by external formate.
468 Moreover, formate supplementation to STM WT enhanced bacterial killing. Cytoplasmic pH
469 analysis using BCECF-AM staining after 72 hours revealed that surviving bacteria—regardless
470 of formate exposure—shared similar pH levels when treated with meropenem. This implies
471 that cytoplasmic pH plays a key role in bacterial survival under antibiotic stress, and that
472 surviving bacteria may carry mutations allowing pH regulation, although characterizing these
473 mutations was beyond the scope of this study and warrants future investigation.
474 Overall, the effectiveness of antibiotics is closely tied to the metabolic state of bacteria, with
475 certain pathways being linked to specific resistance profiles. Mapping these pathways and
476 targeting them with selective inhibitors that shift the metabolic state of resistant bacteria toward
477 that of susceptible ones could offer a promising strategy to combat antibiotic resistance.
478

479 **Acknowledgements**

480 We thank the Departmental Real-Time PCR, Divisional Mass Spectrometry, Divisional Flow
481 Cytometry Facility, Divisional Atomic Force Microscopy, and the Central Animal Facility at
482 IISc for supporting experimental work. Dr. Sunitha assisted in formate quantification via GC-
483 MS. Flow cytometry data acquisition was supported by Mr. Munish and Mrs. Navya. Atomic
484 Force Microscopy was supported by Mrs. Monisha.
485

Author Contributions

DM and DC conceived the study and designed the experiments. DM conducted all experiments, data acquisition, analysis, figure preparation, and wrote the original draft. SVW, PG, and AB helped DM with experiments. DM and DC contributed to manuscript editing. DC supervised the project and secured funding. All authors reviewed and approved the final manuscript.

Declaration of Interest

The authors declare no conflicts of interest.

Funding Information

We gratefully acknowledge financial support from the Department of Biotechnology (DBT) and the Department of Science and Technology (DST), Ministry of Science and Technology. DC thanks DAE for the SRC Outstanding Investigator Award, ASTRA Chair Professorship, and TATA Innovation Fellowship. Additional support came from the DBT-IISc Partnership Program. Infrastructure support from ICMR (Molecular Medicine Center), DST (FIST), and UGC-CAS is also acknowledged. DM is supported by IISc fellowship. PG is supported by DBT-JRF fellowship. AB acknowledges UGC fellowship. The funders had no involvement in study design, data collection, analysis, or publication decisions.

Data Availability

Data supporting this study are available from the authors upon request.

Figure legends

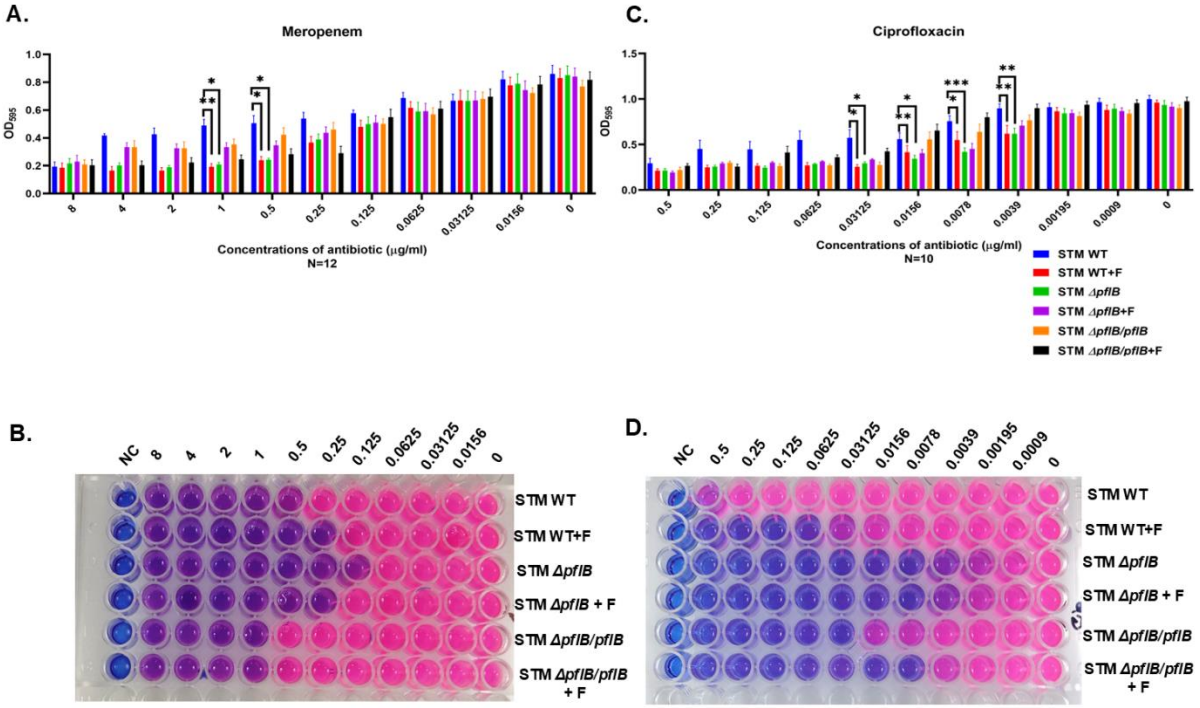

Figure 1

Figure 1: Deletion of *pflB* increases STM's sensitivity to meropenem and ciprofloxacin, while extracellular formate supplementation similarly enhances antibiotic susceptibility.

Meropenem and ciprofloxacin susceptibility of STM WT, STM Δ*pflB*, and STM Δ*pflB*/pQE60: *pflB*, with or without formate treatment, was assessed using the microfold dilution method (A, C) and the resazurin assay (B, D).

(Unpaired two-tailed Student's t-test for column graphs, Two-way Anova for grouped data, Mann-Whitney U-test for animal experiment data (*** $p < 0.0001$, *** $p < 0.001$, ** $p<0.01$, * $p<0.05$))

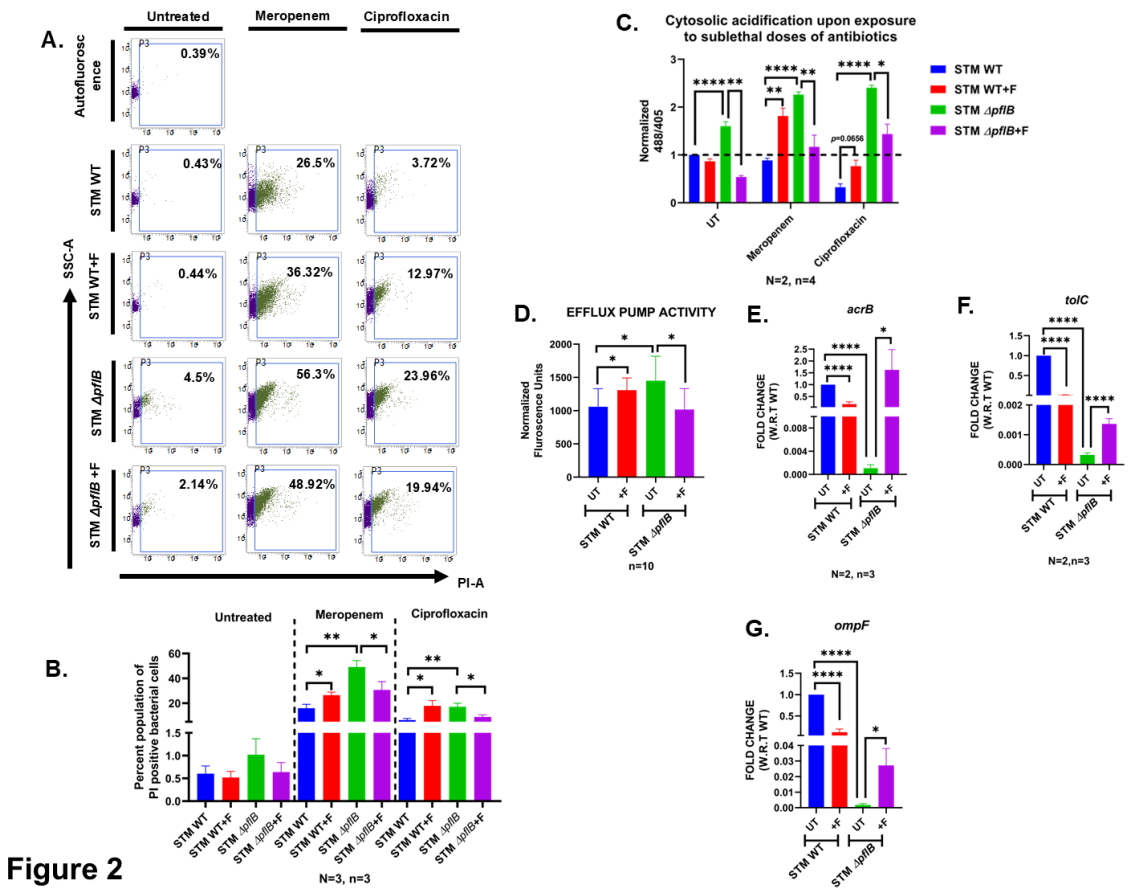

Figure 2

Figure 2: Increased antibiotic sensitivity following *pflB* deletion was linked to transcriptional downregulation of efflux pumps, a pattern also observed in formate-treated wild-type cells.

Dot plots (SSC-A vs PI-A) and bar graphs (A, B) illustrate increased bacterial killing with meropenem and ciprofloxacin following *pflB* deletion and formate supplementation in STM WT. BCECF dye analysis shows disrupted cytosolic pH in STM Δ*pflB* under antibiotic stress, which is restored by exogenous formate (C). Nile red assay quantifies efflux pump activity (D), while transcript levels of *acrB*, *tolC*, and *ompF* are measured in STM WT and STM Δ*pflB*, with or without formate treatment (E, F, G).

(Unpaired two-tailed Student's t-test for column graphs, Two-way Anova for grouped data, Mann-Whitney U-test for animal experiment data (*** $p < 0.0001$, *** $p < 0.001$, ** $p<0.01$, * $p<0.05$))

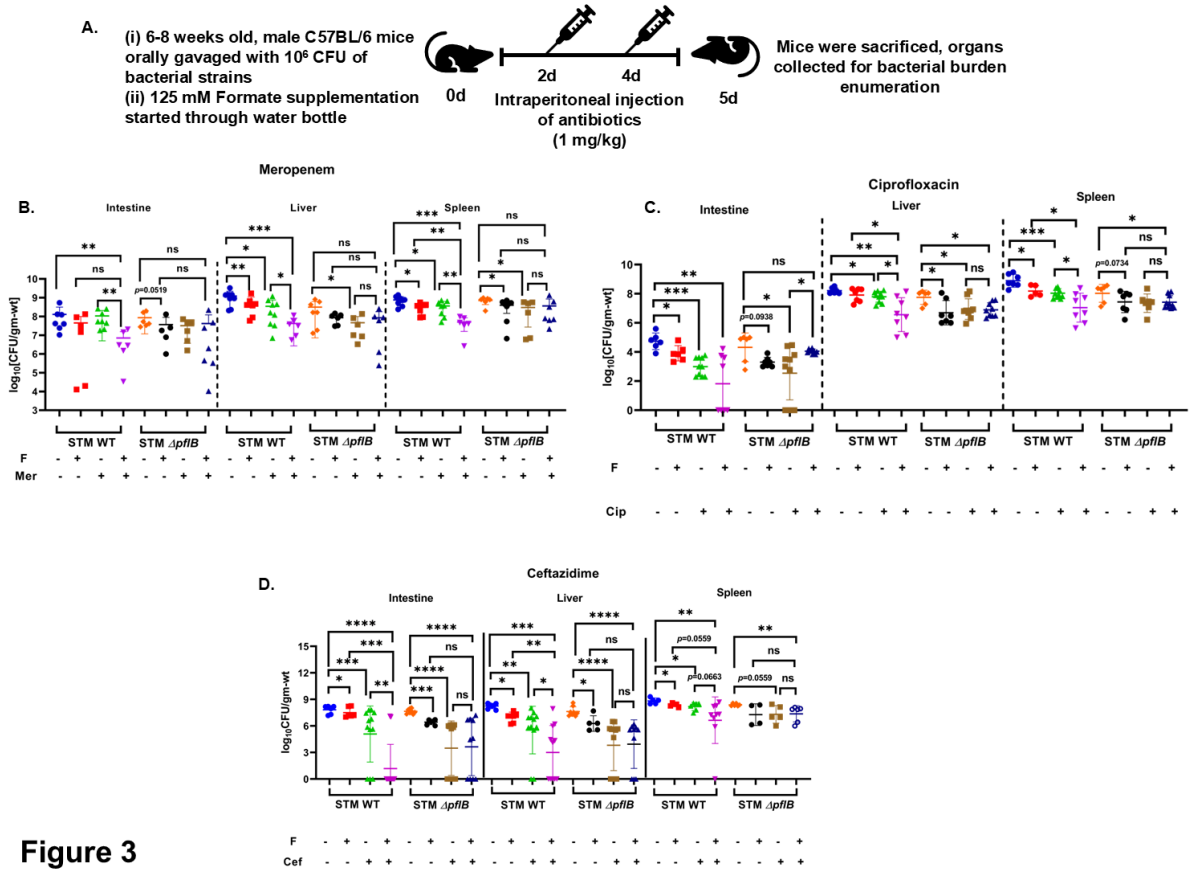

Figure 3

Figure 3: Both formate supplementation via drinking water and internal formate deficiency enhanced antibiotic-mediated bacterial clearance *in vivo*.

Schematic outlining the experimental design (A). Formate supplementation improved STM WT clearance from the intestine, liver, and spleen following treatment with meropenem (B), ciprofloxacin (C), and ceftazidime (D). STM Δ*pflB* showed increased *in vivo* killing upon antibiotic treatment, while exogenous formate helped maintain its bacterial load in mice (B, C, D).

(Unpaired two-tailed Student's t-test for column graphs, Two-way Anova for grouped data, Mann-Whitney U-test for animal experiment data (*** $p < 0.0001$, *** $p < 0.001$, ** $p<0.01$, * $p<0.05$))

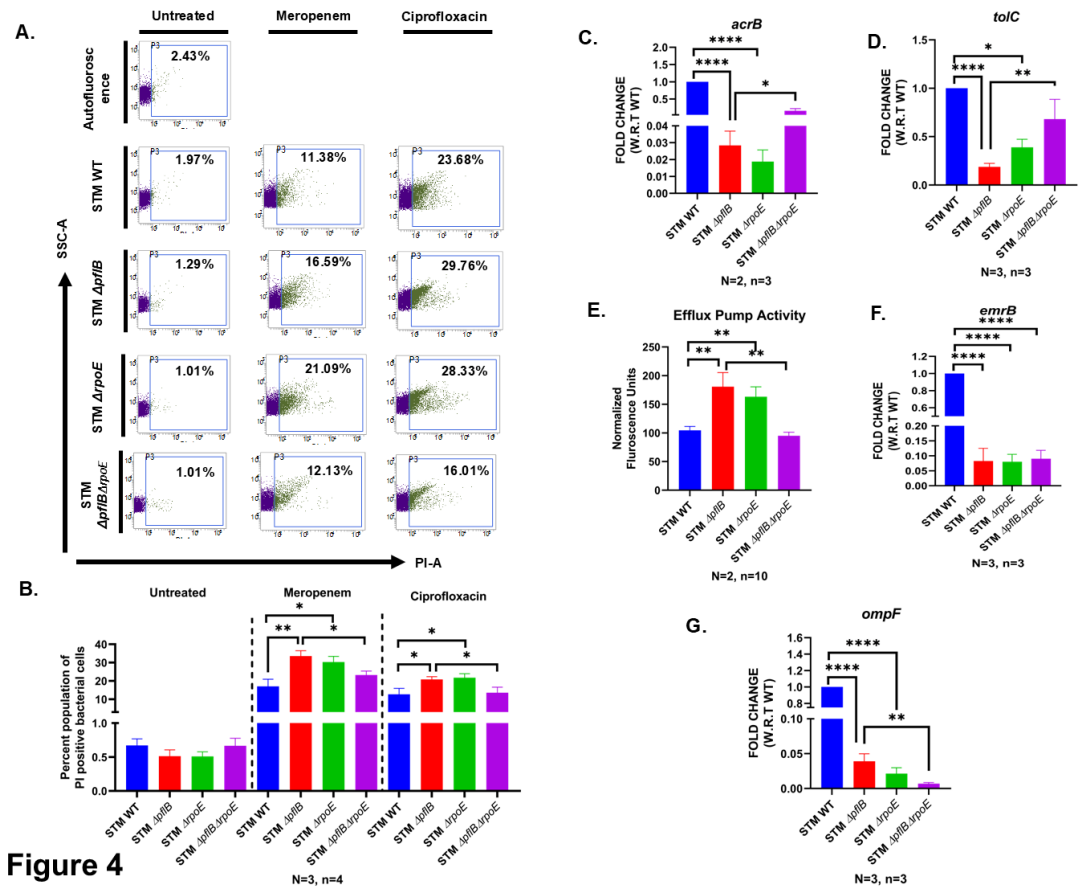

Figure 4

Figure 4: Deletion of *rpoE* in STM Δ*pflB* reversed its increased antibiotic sensitivity, accompanied by restored *acrB* and *tolC* transcript levels.

Dot plots (SSC-A vs PI-A) and bar graphs (A, B) show reduced antibiotic-mediated killing in STM Δ*pflB* upon *rpoE* deletion. Transcript levels of key efflux pump genes *acrB* and *tolC* were compared between STM Δ*pflB*Δ*rpoE* and STM Δ*pflB* (C, D). Efflux activity was assessed using the Nile red assay (E), and expression of *emrB* and *ompF* was also evaluated (F, G). (Unpaired two-tailed Student's t-test for column graphs, Two-way Anova for grouped data, Mann-Whitney U-test for animal experiment data (*** $p < 0.0001$, *** $p < 0.001$, ** $p<0.01$, * $p<0.05$))

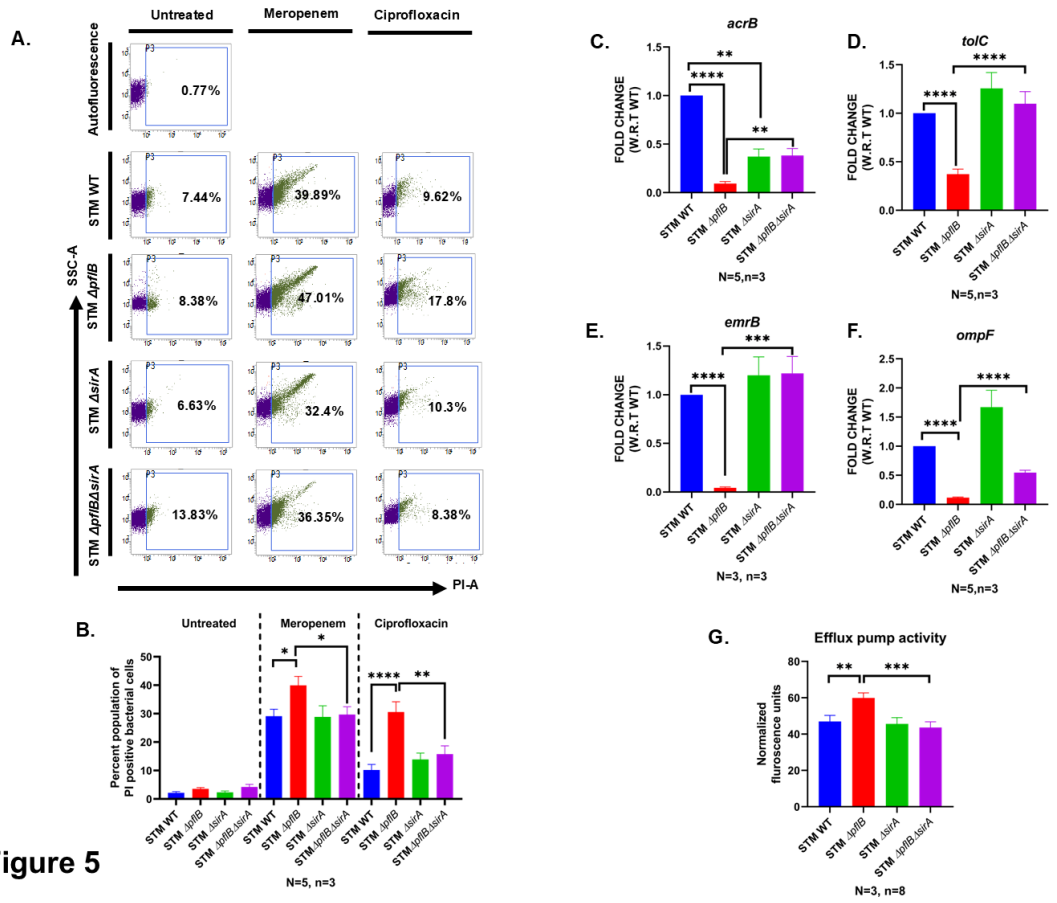

Figure 5

Figure 5: Deleting *sirA* in STM Δ*pflB* similarly reversed its heightened antibiotic sensitivity and restored *acrB* and *tolC* expression levels.

Dot plots (SSC-A vs PI-A) and bar graphs (A, B) show reduced antibiotic-mediated killing in STM Δ*pflB* upon *sirA* deletion. Transcript levels of efflux pump genes *acrB, tolC*, *emrB,* and *ompF* were compared between STM Δ*pflB*Δ*sirA* and STM Δ*pflB* (C, D, E, F). Efflux activity was assessed using the Nile red assay (G).

(Unpaired two-tailed Student's t-test for column graphs, Two-way Anova for grouped data, Mann-Whitney U-test for animal experiment data (*** $p < 0.0001$, *** $p < 0.001$, ** $p<0.01$, * $p<0.05$))

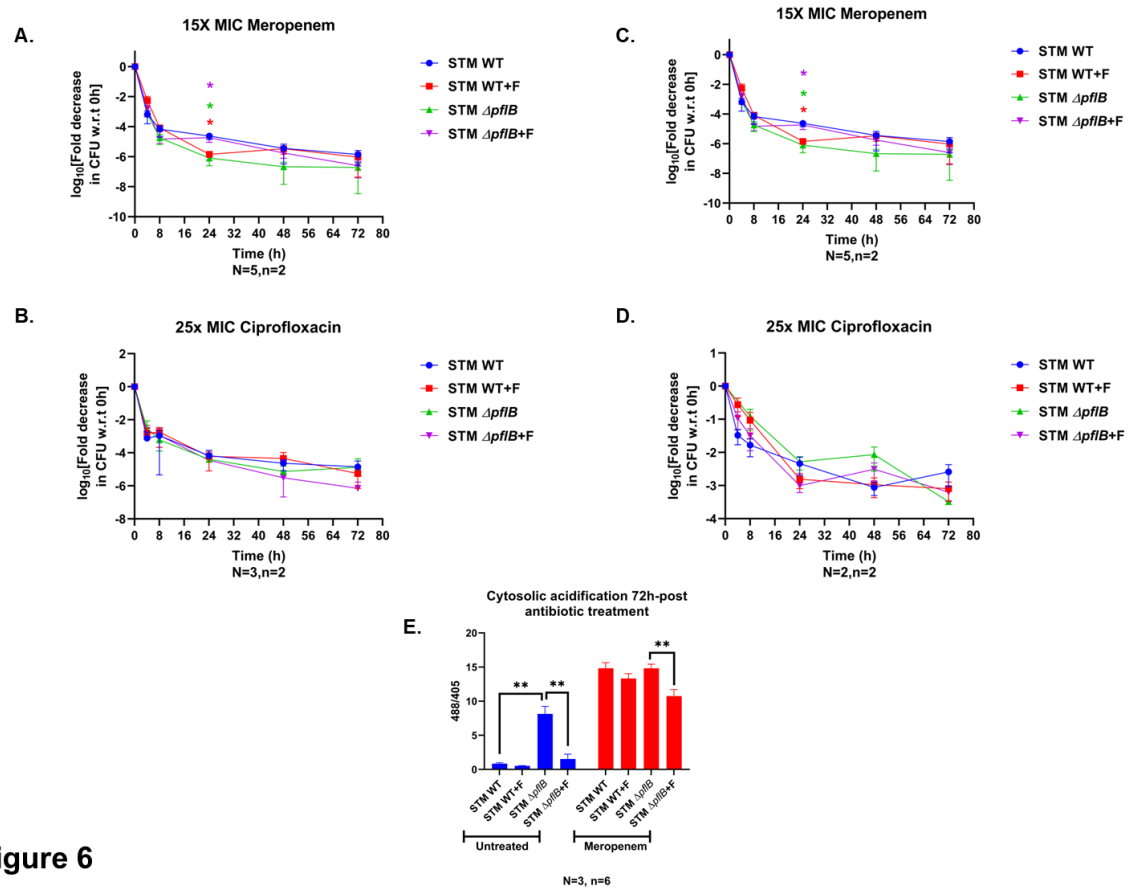

Figure 6

Figure 6: Deletion of *pflB* reduced STM's long-term survival under high antibiotic concentrations, an effect also seen with formate supplementation in the wild type.

Line graphs show $\log_{10}$ fold reduction in CFU relative to 0h for planktonic (A, B) and biofilm (C, D) cultures of STM WT and STM Δ*pflB*, with or without formate supplementation, following exposure to high doses of meropenem and ciprofloxacin at 4, 8, 24, 48, and 72 hours. BCECF staining was performed on 72h colonies, with or without meropenem treatment (E).

(Unpaired two-tailed Student's t-test for column graphs, Two-way Anova for grouped data, Mann-Whitney U-test for animal experiment data (*** $p < 0.0001$, *** $p < 0.001$, ** $p<0.01$, * $p<0.05$))

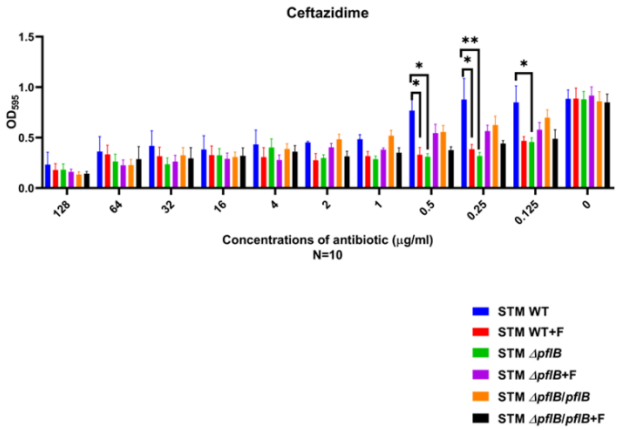

Figure S1

Figure S1: Deletion of *pflB* increases STM's susceptibility to the third-generation cephalosporin ceftazidime, and similar sensitivity is observed with extracellular formate supplementation.

Ceftazidime susceptibility in STM WT, STM Δ*pflB*, and STM Δ*pflB*/pQE60:*pflB*, with or without formate, was evaluated using the microfold dilution method.

(Unpaired two-tailed Student's t-test (column graphs), two-way ANOVA (grouped data), and Mann–Whitney U-test (animal data).

(***$p < 0.0001$, **$p < 0.001$, **$p < 0.01$, *$p < 0.05$))

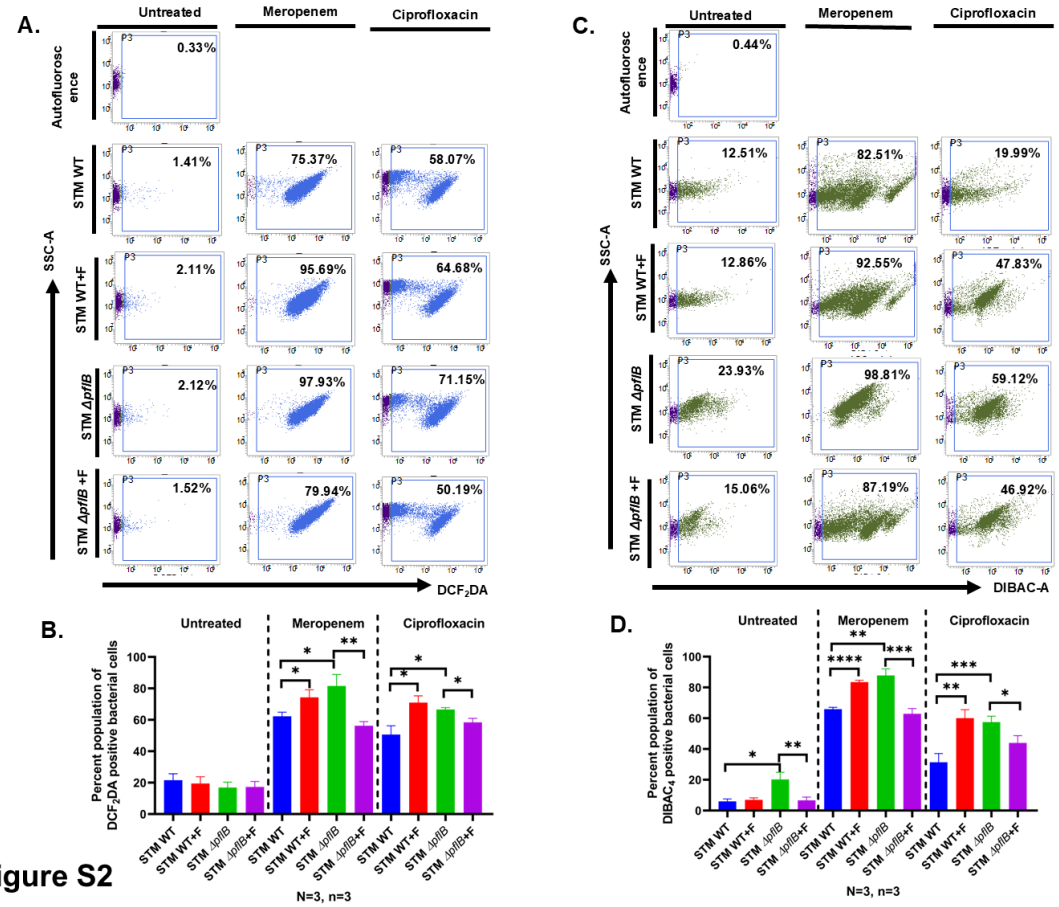

Figure S2

Figure S2: Enhanced antibiotic sensitivity due to *pflB* deletion correlates with increased DCF2DA and DiBAC4 staining, indicating elevated ROS levels and membrane depolarization—effects also seen in formate-treated STM WT. Dot plots (SSC-A vs DCF_2DA/DiBAC-A) (A, C) and corresponding bar graphs (B, D) show higher intracellular ROS and membrane depolarization following meropenem and ciprofloxacin treatment in STM ΔpflB and formate-supplemented STM WT. (Unpaired two-tailed Student's t-test (column graphs), two-way ANOVA (grouped data), and Mann–Whitney U-test (animal data).

(***$p < 0.0001$, **$p < 0.001$, **$p < 0.01$, *$p < 0.05$))

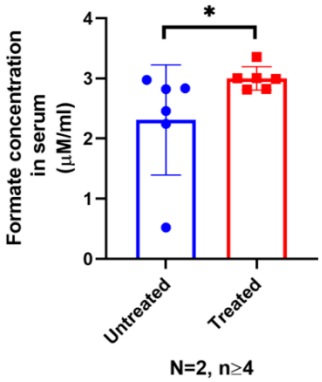

Figure S3

Figure S3: Formate supplementation increased formate levels in serum of treated mice

Bar graph showing formate levels in mice serum after exposure to formate through drinking water

(Unpaired two-tailed Student's t-test (column graphs), two-way ANOVA (grouped data), and Mann–Whitney U-test (animal data).

(***$p < 0.0001$, **$p < 0.001$, **$p < 0.01$, *$p < 0.05$))

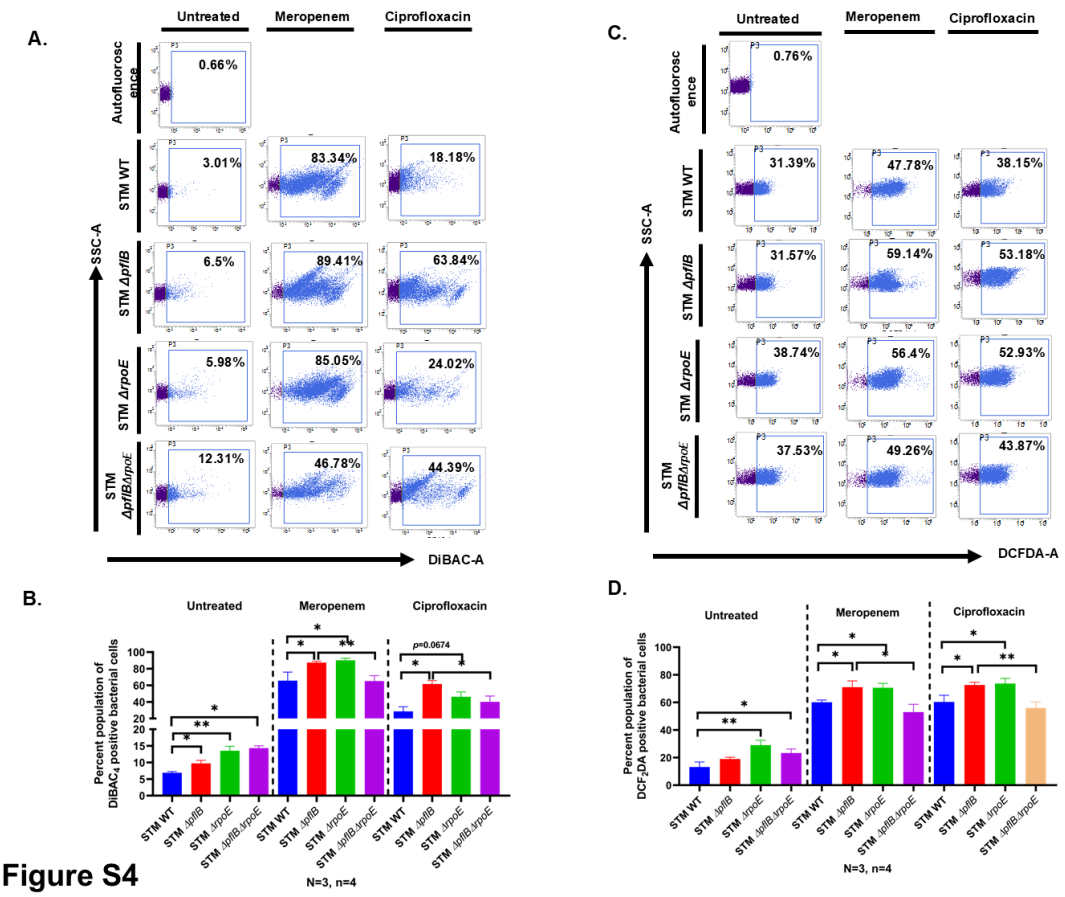

Figure S4

Figure S4: Recovered antibiotic sensitivity due to *rpoE* deletion in STM Δ*pflB* correlates with reduced intracellular ROS levels but it did not have any effect on membrane depolarization

Dot plots (SSC-A vs DIBAC-A/ DCF_2DA) (A, C) and corresponding bar graphs (B, D) compares intracellular ROS and membrane depolarization following meropenem and ciprofloxacin treatment in STM Δ*pflB* and STM Δ*pflB*Δ*rpoE*.

(Unpaired two-tailed Student's t-test (column graphs), two-way ANOVA (grouped data), and Mann–Whitney U-test (animal data).

(***$p < 0.0001$, **$p < 0.001$, **$p < 0.01$, *$p < 0.05$))

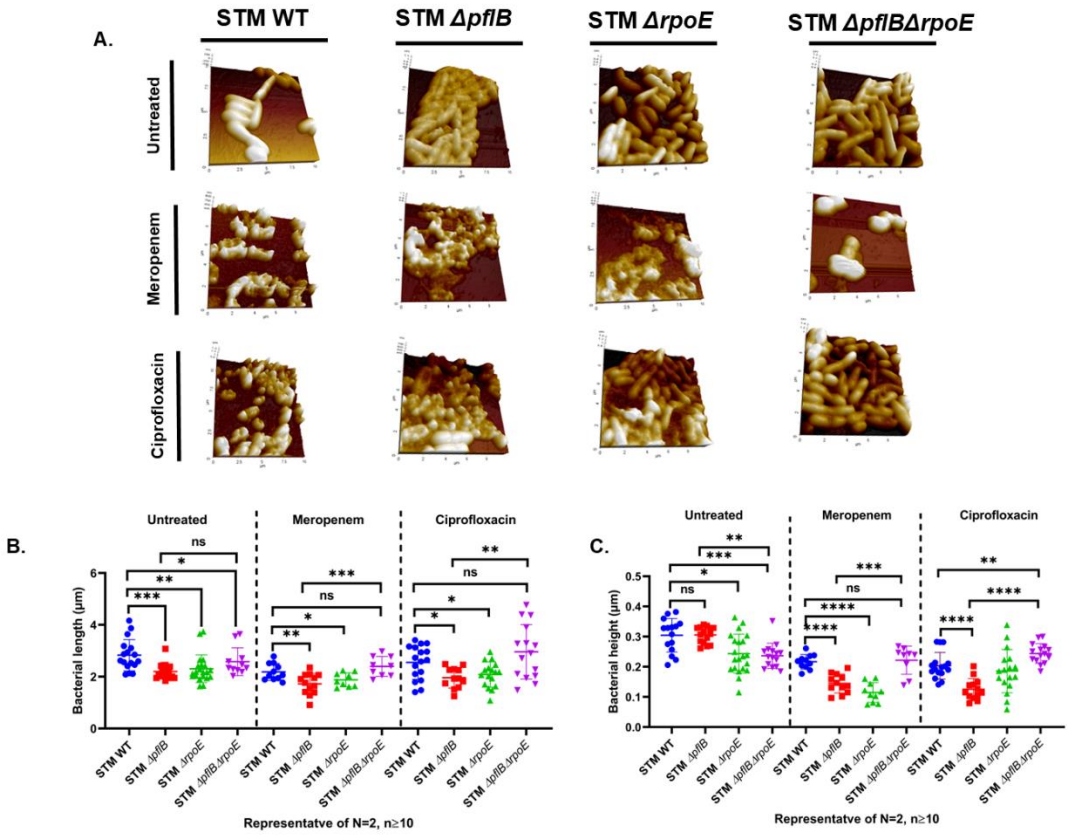

622 **Figure S5**

623 **Figure S5: The recovery in antibiotic sensitivity upon *rpoE* deletion in STM Δ*pflB* was**
624 **also evident from morphological changes under Atomic Force Microscopy**

625 AFM-assissted visualization of morphology of STM WT, STM Δ*pflB*, STM Δ*rpoE*, STM
626 Δ*pflB*Δ*rpoE* upon expsure to sublethal concentrations of meropenem and ciprofloxacin (A) and
627 quantification of bacterial length (B) and height (C) from the same.

628 (Unpaired two-tailed Student's t-test (column graphs), two-way ANOVA (grouped data), and
629 Mann–Whitney U-test (animal data).

630 (***p < 0.0001, **p < 0.001, **p < 0.01, *p < 0.05))

631

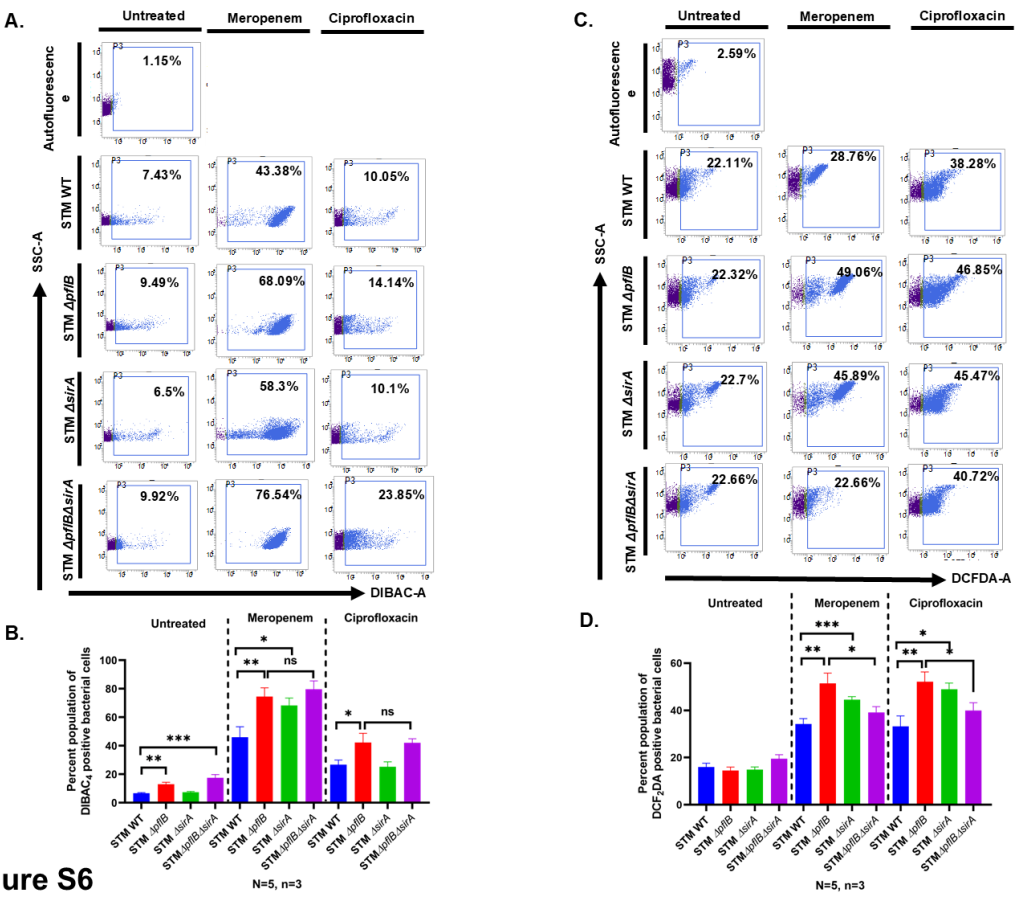

632 **Figure S6**

633 **Figure S6: *sirA* deletion mediated reduction of antibiotic susceptibility in STM Δ*pflB* was**

634 **associated with reduced intracellular ROS levels, but without any effect on membrane**

635 **depolarization**

636 Dot plots (SSC-A vs DIBAC-A/ DCF_2DA) (A, C) and corresponding bar graphs (B, D) shows

637 a comparative analysis between intracellular ROS and membrane depolarization following

638 meropenem and ciprofloxacin treatment in STM Δ*pflB* and STM Δ*pflB*Δ*sirA*.

639

640

641

642

643 **References:**

644 1. Zhu S, Yang B, Jia Y et al. Comprehensive analysis of disinfectants on the horizontal
645 transfer of antibiotic resistance genes. *J Hazard Mater* 2023; **453**: 131428.

2. Brauner A, Fridman O, Gefen O et al. Distinguishing between resistance, tolerance and persistence to antibiotic treatment. *Nat Rev Microbiol* 2016; **14**: 320-30.
3. Antimicrobial Resistance C. Global burden of bacterial antimicrobial resistance in 2019: a systematic analysis. *Lancet* 2022; **399**: 629-55.
4. Azmatullah A, Qamar FN, Thaver D et al. Systematic review of the global epidemiology, clinical and laboratory profile of enteric fever. *J Glob Health* 2015; **5**: 020407.
5. Kim TH, Hwang HJ, Kim JH. Development of a Novel, Rapid Multiplex Polymerase Chain Reaction Assay for the Detection and Differentiation of Salmonella enterica Serovars Enteritidis and Typhimurium Using Ultra-Fast Convection Polymerase Chain Reaction. *Foodborne Pathog Dis* 2017; **14**: 580-6.
6. Zhang H, Yao S, Sheng R et al. A cascade amplification strategy for ultrasensitive Salmonella typhimurium detection based on DNA walker coupling with CRISPR-Cas12a. *J Colloid Interface Sci* 2022; **625**: 257-63.
7. Wu S, Ji J, Sheng L et al. Lysine and valine weaken antibiotic resistance in Salmonella Typhimurium induced by disinfectant stress. *J Hazard Mater* 2024; **480**: 135858.
8. Punchihewage-Don AJ, Ranaweera PN, Parveen S. Defense mechanisms of Salmonella against antibiotics: a review. *Front Antibiot* 2024; **3**: 1448796.
9. Chowdhury AR, Mukherjee D, Chatterjee R et al. Defying the odds: Determinants of the antimicrobial response of Salmonella Typhi and their interplay. *Mol Microbiol* 2024; **121**: 213-29.
10. Mukherjee D, Chakravortty D. A Tale of Twins: The Distinct Roles of Intracellular and Extracellular Formate in Regulating Flagellar and Pathogenicity Island-1 Genes in Salmonella Typhimurium. *bioRxiv* 2024: 2024.01.30.577997.
11. Lyu Z, Yang A, Villanueva P et al. Heterogeneous Flagellar Expression in Single Salmonella Cells Promotes Diversity in Antibiotic Tolerance. *mBio* 2021; **12**: e0237421.
12. Chowdhury AR, Mukherjee D, Singh AK et al. Loss of outer membrane protein A (OmpA) impairs the survival of Salmonella Typhimurium by inducing membrane damage in the presence of ceftazidime and meropenem. *J Antimicrob Chemother* 2022; **77**: 3376-89.
13. Hughes ER, Winter MG, Duerkop BA et al. Microbial Respiration and Formate Oxidation as Metabolic Signatures of Inflammation-Associated Dysbiosis. *Cell Host Microbe* 2017; **21**: 208-19.
14. Drescher SPM, Gallo SW, Ferreira PMA et al. Salmonella enterica persister cells form unstable small colony variants after in vitro exposure to ciprofloxacin. *Sci Rep* 2019; **9**: 7232.
15. Papich MG. Saunders handbook of veterinary drugs. *North Carolina* 2016; **12**: 162-71.
16. Dwyer DJ, Kohanski MA, Hayete B et al. Gyrase inhibitors induce an oxidative damage cellular death pathway in Escherichia coli. *Mol Syst Biol* 2007; **3**: 91.
17. Kohanski MA, Dwyer DJ, Hayete B et al. A common mechanism of cellular death induced by bactericidal antibiotics. *Cell* 2007; **130**: 797-810.
18. Dwyer DJ, Belenky PA, Yang JH et al. Antibiotics induce redox-related physiological alterations as part of their lethality. *Proc Natl Acad Sci U S A* 2014; **111**: E2100-9.
19. Reyes-Fernandez EZ, Schuldiner S. Acidification of Cytoplasm in Escherichia coli Provides a Strategy to Cope with Stress and Facilitates Development of Antibiotic Resistance. *Sci Rep* 2020; **10**: 9954.
20. Panta PR, Doerrler WT. A link between pH homeostasis and colistin resistance in bacteria. *Sci Rep* 2021; **11**: 13230.
21. Roy Chowdhury A, Sah S, Varshney U et al. Salmonella Typhimurium outer membrane protein A (OmpA) renders protection from nitrosative stress of macrophages by maintaining the stability of bacterial outer membrane. *PLoS Pathog* 2022; **18**: e1010708.
22. Epand RF, Pollard JE, Wright JO et al. Depolarization, bacterial membrane composition, and the antimicrobial action of ceragenins. *Antimicrob Agents Chemother* 2010; **54**: 3708-13.
23. Te Winkel JD, Gray DA, Seistrup KH et al. Analysis of Antimicrobial-Triggered Membrane Depolarization Using Voltage Sensitive Dyes. *Front Cell Dev Biol* 2016; **4**: 29.

24. Han FF, Gao YH, Luan C et al. Comparing bacterial membrane interactions and antimicrobial activity of porcine lactoferricin-derived peptides. *J Dairy Sci* 2013; **96**: 3471-87.
25. Soren O, Brinch KS, Patel D et al. Antimicrobial Peptide Novicidin Synergizes with Rifampin, Ceftriaxone, and Ceftazidime against Antibiotic-Resistant Enterobacteriaceae In Vitro. *Antimicrob Agents Chemother* 2015; **59**: 6233-40.
26. Cheng M, Huang JX, Ramu S et al. Ramoplanin at bactericidal concentrations induces bacterial membrane depolarization in Staphylococcus aureus. *Antimicrob Agents Chemother* 2014; **58**: 6819-27.
27. Masi M, Refregiers M, Pos KM et al. Mechanisms of envelope permeability and antibiotic influx and efflux in Gram-negative bacteria. *Nat Microbiol* 2017; **2**: 17001.
28. Du D, Wang-Kan X, Neuberger A et al. Multidrug efflux pumps: structure, function and regulation. *Nat Rev Microbiol* 2018; **16**: 523-39.
29. Ramaswamy VK, Vargiu AV, Malloci G et al. Molecular Rationale behind the Differential Substrate Specificity of Bacterial RND Multi-Drug Transporters. *Sci Rep* 2017; **7**: 8075.
30. Rosenberg EY, Ma D, Nikaido H. AcrD of Escherichia coli is an aminoglycoside efflux pump. *J Bacteriol* 2000; **182**: 1754-6.
31. Webber MA, Bailey AM, Blair JM et al. The global consequence of disruption of the AcrAB-TolC efflux pump in Salmonella enterica includes reduced expression of SPI-1 and other attributes required to infect the host. *J Bacteriol* 2009; **191**: 4276-85.
32. Ziervogel BK, Roux B. The binding of antibiotics in OmpF porin. *Structure* 2013; **21**: 76-87.
33. Choi KM, Kim MH, Cai H et al. Salicylic Acid Reduces OmpF Expression, Rendering Salmonella enterica Serovar Typhimurium More Resistant to Cephalosporin Antibiotics. *Chonnam Med J* 2018; **54**: 17-23.
34. Dhayade S, Pietzke M, Wiesheu R et al. Impact of Formate Supplementation on Body Weight and Plasma Amino Acids. *Nutrients* 2020; **12**.
35. Ricci V, Attah V, Overton T et al. CsrA maximizes expression of the AcrAB multidrug resistance transporter. *Nucleic Acids Res* 2017; **45**: 12798-807.
36. Gu Y, Huang L, Wu C et al. The Evolution of Fluoroquinolone Resistance in Salmonella under Exposure to Sub-Inhibitory Concentration of Enrofloxacin. *Int J Mol Sci* 2021; **22**.
37. Salvail H, Groisman EA. The phosphorelay BarA/SirA activates the non-cognate regulator RcsB in Salmonella enterica. *PLoS Genet* 2020; **16**: e1008722.
38. Nava-Galeana J, Nunez C, Bustamante VH. Proteomic analysis reveals the global effect of the BarA/SirA-Csr regulatory cascade in Salmonella Typhimurium grown in conditions that favor the expression of invasion genes. *J Proteomics* 2023; **286**: 104960.
39. Gudapaty S, Suzuki K, Wang X et al. Regulatory interactions of Csr components: the RNA binding protein CsrA activates csrB transcription in Escherichia coli. *J Bacteriol* 2001; **183**: 6017-27.
40. Huemer M, Mairpady Shambat S, Brugger SD et al. Antibiotic resistance and persistence-Implications for human health and treatment perspectives. *EMBO Rep* 2020; **21**: e51034.
41. Algarni S, Ricke SC, Foley SL et al. The Dynamics of the Antimicrobial Resistance Mobilome of Salmonella enterica and Related Enteric Bacteria. *Front Microbiol* 2022; **13**: 859854.
42. Dyson ZA, Klemm EJ, Palmer S et al. Antibiotic Resistance and Typhoid. *Clin Infect Dis* 2019; **68**: S165-S70.
43. Wu S, Yang Y, Wang T et al. Effects of acid, alkaline, cold, and heat environmental stresses on the antibiotic resistance of the Salmonella enterica serovar Typhimurium. *Food Research International* 2021; **144**: 110359.
44. Kuang X, Hao H, Dai M et al. Serotypes and antimicrobial susceptibility of Salmonella spp. isolated from farm animals in China. *Front Microbiol* 2015; **6**: 602.
45. Kebede A, Kemal J, Alemayehu H et al. Isolation, Identification, and Antibiotic Susceptibility Testing of Salmonella from Slaughtered Bovines and Ovines in Addis Ababa Abattoir Enterprise, Ethiopia: A Cross-Sectional Study. *Int J Bacteriol* 2016; **2016**: 3714785.

46. Christou A, Aguera A, Bayona JM et al. The potential implications of reclaimed wastewater reuse for irrigation on the agricultural environment: The knowns and unknowns of the fate of antibiotics and antibiotic resistant bacteria and resistance genes - A review. *Water Res* 2017; **123**: 448-67.
47. Sunuwar J, Azad RK. A machine learning framework to predict antibiotic resistance traits and yet unknown genes underlying resistance to specific antibiotics in bacterial strains. *Brief Bioinform* 2021; **22**.
48. Devanga Ragupathi NK, Muthuirulandi Sethuvel DP, Shankar BA et al. Draft genome sequence of bla(TEM-1)-mediated cephalosporin-resistant Salmonella enterica serovar Typhi from bloodstream infection. *J Glob Antimicrob Resist* 2016; **7**: 11-2.
49. Greninger AL, Chatterjee SS, Chan LC et al. Whole-Genome Sequencing of Methicillin-Resistant Staphylococcus aureus Resistant to Fifth-Generation Cephalosporins Reveals Potential Non-mecA Mechanisms of Resistance. *PLoS One* 2016; **11**: e0149541.
50. Palzkill T. Structural and Mechanistic Basis for Extended-Spectrum Drug-Resistance Mutations in Altering the Specificity of TEM, CTX-M, and KPC beta-lactamases. *Front Mol Biosci* 2018; **5**: 16.
51. Sanders CC. beta-Lactamase stability and in vitro activity of oral cephalosporins against strains possessing well-characterized mechanisms of resistance. *Antimicrob Agents Chemother* 1989; **33**: 1313-7.
52. Ji J, Wu S, Sheng L et al. Metabolic reprogramming of the glutathione biosynthesis modulates the resistance of Salmonella Derby to ceftriaxone. *iScience* 2023; **26**: 107263.
53. Wu S, Ji J, Carole NVD et al. Combined metabolomics and transcriptomics analysis reveals the mechanism of antibiotic resistance of Salmonella enterica serovar Typhimurium after acidic stress. *Food Microbiol* 2023; **115**: 104328.
54. Kitzenberg DA, Lee JS, Mills KB et al. Adenosine Awakens Metabolism to Enhance Growth-Independent Killing of Tolerant and Persister Bacteria across Multiple Classes of Antibiotics. *mBio* 2022; **13**: e0048022.